JCTC Journal of Chemical Theory and Computation

Article

pubs.acs.org/JCTC

Suitability of the MARTINI Force Field for Use with Gas-Phase Protein Complexes

Sarah K. Fegan and Mark Thachuk*

Department of Chemistry, University of British Columbia, 2036 Main Mall, Vancouver, BC, V6T 1Z1, Canada

ABSTRACT: The MARTINI coarse-grained force field [Monticelli, L. et al. *J. Chem. Theory Comput.* **2008**, *4*, 819−834] is examined for use in molecular dynamics simulations of the dissociation of gas-phase protein complexes. Coarse-grained force fields allow longer time scales and larger systems to be treated compared with all-atom force fields. In this work, results for the dissociation of the cytochrome c′ dimer using MARTINI are compared with published studies using the OPLS-AA/L all-atom force field. Several structural parameters such as the minimum distance between monomers, radius of gyration, and root-mean-square deviation as well as potential energy contributions (Lennard-Jones and Coulomb) are calculated as a function of the center of mass distance. The MARTINI force field semiquantitatively reproduces the results of previous all-atom studies but appears to be somewhat too attractive.

INTRODUCTION

Mass spectrometry experiments examining the dissociation of gas-phase protein complexes have been performed by several groups,[1−10] and a recent review[11] details nicely the use of mass spectrometry techniques for studying such complexes. Asymmetric dissociation has been observed for collisionally activated dissociation of several large protein complexes.[2,5,7,10] Asymmetric dissociation in this context means the fragments have different mass to charge ratios. Asymmetric dissociation has also been observed when homodimers are dissociated using collisionally activated dissociation methods.[6] For many cases, the asymmetric dissociation channel is the preferred one when large complexes are fragmented, and this can limit information about other interactions in the complex. Through a better understanding of the dissociation mechanism, it might be possible to control it, leading to experiments which give more structural information.

In addition to experimental work, some theoretical work has also been done to explore the dissociation mechanism. Klassen and co-workers[9] used the charged droplet model and a protein structure model to calculate energies for a single subunit leaving a pentamer. Their protein structure model used more detailed structural information but assumed that the displacement of one monomer was the only change in the structure on dissociation. Their results show that protein unfolding may be important to the asymmetric charge distribution, and a simple Coulomb energy calculation is useful in understanding the dissociation. Experimental evidence for protein unfolding had already been presented by Williams and Jurchen.[6]

Konermann and co-workers[12] used a simple model where folded proteins were represented by spheres and unfolded proteins by a string of smaller spheres. The number of beads used for the unfolded proteins was varied to model partial as well as fully unfolded proteins. They found that dimers dissociating without unfolding had a symmetric charge distribution, while when one of the subunits unfolded the charge distribution was asymmetric. An asymmetric charge partitioning was also found when one unit of a tetramer unfolded while the other three remained folded. Their study also included collision-induced dissociation mass spectrometry experiments of dimer and tetramer proteins. By comparing the experimental spectra to the charge distributions predicted by the model, they concluded that dissociation was occurring with a range of structures having varying degrees of unfolding.

The work by Csiszar and Thachuk[13] used charged ellipsoids to model surface charges. They found that a constant surface charge density was the most favorable distribution. So for a dimer with an asymmetric charge partitioning, the monomer with more charges would want to unfold to have a surface area larger than that of the monomer with fewer charges. All-atom studies were performed by Wanasundara and Thachuk[14−16] on the dissociation of cytochrome c′ dimers. Their work showed that the symmetric case with +5 charges on each monomer had a lower barrier to dissociation than the neutral dimer, and the asymmetric cases (M8/M2 and M9/M1) had higher barriers. The higher charged monomers in the asymmetric cases unfolded while the lower charged monomers remained folded. The difficulty with all-atom simulations is that they are not practical for simulating long times or large systems. We would like to simulate protein complexes larger than dimers, and we would also like to be able to include charge hopping.

Coarse-grained models use interaction sites that represent groups of atoms rather than explicitly including all of the atoms in a molecule. See for example the review article by Tozzini.[17] By reducing the number of particles in the simulation and removing the light atoms which have fast vibrations, coarse-grained models are computationally faster than all-atom models. One type of coarse-graining is the united atom model (for example, the Amber united atom model[18] and the OPLS united atom model[19]). These have the hydrogen atoms included with the heavy atom to which they are bonded, but each heavy atom is represented by a single interaction site. They are faster than all-atom models but not as fast as some

Received: October 21, 2011
Published: March 7, 2012

coarser models. At the other end of the coarseness scale are models that use one or two beads for each amino acid. These models like the Go model[20,21] are usually parametrized to reproduce the correct folding for a particular protein and are difficult to transfer to proteins with different structures.

For this study, the MARTINI force field[22,23] was employed. It uses one bead for an average of four heavy atoms, so one to four beads are used for each amino acid. It has been implemented for the GROMACS software package,[24−26] and files with the necessary parameters are readily available. The MARTINI force field was originally created for lipids.[22] It was parametrized on the basis of thermodynamic properties such as free energies of hydration, vaporization, and water/organic solvent partitioning. Baron and co-workers[27−29] compared thermodynamic properties from all-atom and coarse-grained simulations. The coarse-grained model they used was an older version of MARTINI. They found the coarse-grained systems had a lower entropy than the corresponding all-atom systems, but the major structural features were similar. Monticelli et al. then extended the MARTINI force field to include proteins.[23] It was successfully used in several studies.[30−33] Simulations of a series of peptides at an interface were used to calculate partitioning free energies which were compared to experimental data.[34] Milani and co-workers used a modified MARTINI force field to study isolated nanofibers.[35] Their results were consistent with experimental results.

Since this force field was parametrized with molecules in solution, it is necessary to validate the force field for use in the gas phase. The goal of the present study is to use the MARTINI force field to replicate the all-atom studies[14−16] and compare the results, thereby assessing its utility for further gas-phase simulations.

METHOD

The system used for this study is the cytochrome c′ dimer (PDB ID: 1bbh).[36] Molecular dynamics simulations were performed using GROMACS version 4.0.7[24−26] with the MARTINI version 2.1 coarse-grained force field.[22,23] The temperature was kept constant at 300 K using the Nosé−Hoover thermostat.[37] Because this system is an isolated molecule without solvent, no periodic boundary conditions were used. The absence of solvent also means that charges and intermolecular interactions are unattenuated, so for the Lennard-Jones and Coulomb electrostatics no cutoffs or shifts were employed. The default value of the relative dielectric constant used with MARTINI accounts in part for the effect of solvent. In this study, charges residing on dissociating fragments act through empty space, for which a relative dielectric constant of unity is physically appropriate. In principle, charges within a monomer interact through the protein itself and would require a relative dielectric constant different from unity. However, as the protein conformation changes, the relative balance between through-space and through-protein interactions changes in a dynamic manner. Because the through-space contributions are most important for describing correctly the dissociation process, the relative dielectric constant was set to unity for all simulations. All energies are reported in kilojoules per mole and all distances in nanometers.

We consider three partitionings of charges between the two monomers. The first is neutral complexes with no charges. The second has an M5/M5 charge partitioning, being symmetric with five charges on each monomer for a total charge of +10, and the third has an M8/M2 charge partitioning, being asymmetric with eight charges on one monomer and two charges on the other monomer also for a total charge of +10. In each of the positively charged monomers, the charges are distributed among the basic amino acid side chains and the N-terminus. Figure 1 shows the positions of the basic amino acids

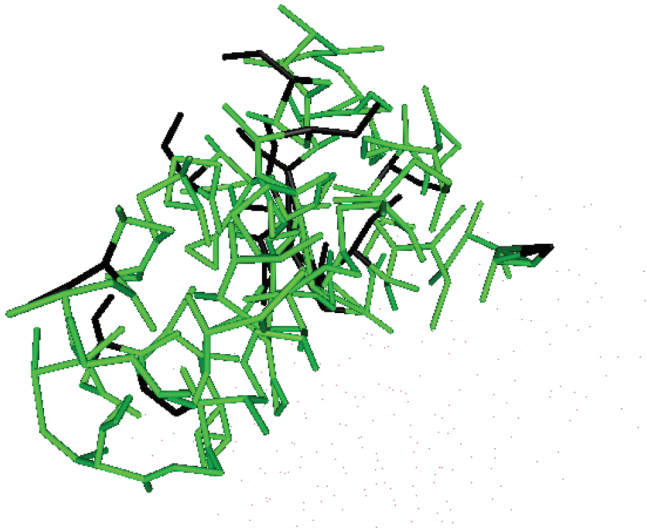

Figure 1. Snapshot of a ground state monomer showing the available basic amino acid residues (and the N-terminus) in black and the other amino acids in green.

available for the positive charges. All of the charges are fixed, and no partial charges are used. The charged beads were modified to the MARTINI Qd type. The same 10 charge distributions are used for each of the charge partitionings as were used by Wanasundara and Thachuk.[15] They were chosen as the lowest energy configurations based upon short molecular dynamics relaxations. For details of the screening method, see ref 15. The residue numbers of the charged amino acids are listed in Table 1 for each of the 20 charge distributions (residue 1 is the N-terminus). For each charge distribution, 10 trajectories were propagated, for a total of 100 trajectories. The results reported in each case are the averages of these 100 trajectories.

The reaction coordinate used for the dissociation of the dimer is the distance between the centers of mass of each of the monomers. The center of mass (COM) distance for the ground state dimer in the MARTINI force field is 1.4 nm, and in the all-atom study, which employed the OPLS-AA/L force field, the ground state COM distance was 2 nm.[15]

In addition to regularly bonded structures, trajectories were also propagated for these same structures supplemented with local elastic network bonds. Elastic network bonds[38] connect selected backbone beads with harmonic potentials. Topologies can be created with or without elastic network bonds. These bonds, when made between flexible parts of a protein, increase the stability of the protein, thereby allowing a larger time step to be used. Combining elastic network bonds with the MARTINI force field allows for faster simulations than the MARTINI force field alone. The effect of these bonds on the results will be considered.

In the present case, 20 local elastic network bonds were created each with a force constant of 2500 kJ/(mol nm), a value much larger than those for regular bonds. These network

Table 1. The Residue Numbers of the Charged Amino Acids on Each Monomer for the 10 M8/M2 and 10 M5/M5 Charge Distributions

	M8	M2
c1	1 25 27 70 72 74 89 111	64 74
c2	1 25 27 70 72 74 89 111	72 89
c3	1 25 27 70 72 74 89 111	74 89
c4	1 25 27 70 72 74 89 111	74 127
c5	1 25 27 70 72 74 89 111	89 127
c6	1 25 27 70 72 74 89 111	89 131
c7	1 25 27 64 74 89 111 129	89 131
c8	1 25 27 64 70 72 89 111	72 86
c9	1 25 27 64 70 74 89 111	89 129
c10	1 25 64 70 72 74 89 111	72 86
	M5	M5
c1	25 64 72 89 111	25 64 72 89 111
c2	25 64 72 89 111	25 64 74 89 111
c3	25 64 72 89 111	25 64 89 111 131
c4	25 64 72 89 111	25 72 89 111 127
c5	25 64 72 89 111	64 72 89 111 127
c6	25 70 74 89 111	64 74 89 111 129
c7	25 70 74 89 111	25 64 89 111 129
c8	25 70 74 89 111	25 64 72 89 111
c9	25 64 70 89 111	25 64 72 89 111
c10	25 64 74 89 111	64 72 74 89 111

bonds are located in parts of the protein where there are four or more amino acids which have an extended secondary structure (they are not part of a helix or β sheet). The atoms involved in the elastic network bonds are shown in Figure 2. Each

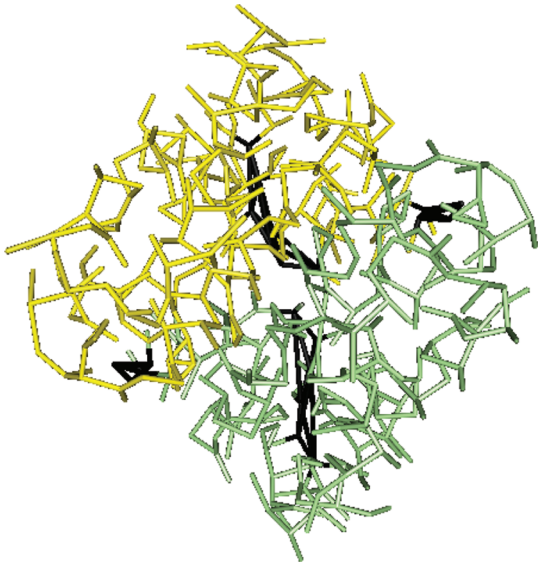

Figure 2. Snapshot of the ground state dimer showing the atoms involved in elastic network bonds in black. One monomer is shown in yellow; the other is shown in green.

monomer has two regions containing elastic network bonds, but each such bond connects atoms only within its region. That is, no elastic network bonds connect atoms between the two regions. For complexes with elastic network bonds, it was possible to use a time step of 30 fs, while the same time step caused instabilities when the elastic bond network was removed. In the latter case, trajectories would propagate without incident for short times but for longer times would reach a point where their energies and temperatures would start to grow uncontrollably. This was traced to a fast motion occurring within the extended structure in which the elastic network was removed. At some point, an event occurs whereby two beads approach too closely (since the time step of 30 fs is too large to correctly account for the fast motion). A bad contact occurs, and the energy increases too rapidly for the thermostat to compensate. This event is rare, but for long simulation times it would occur in approximately 30% of the trajectories. It is possible that these fast motions are a difficulty only for gas-phase calculations where no solvent is present to dampen them. To avoid the problem, the time step was reduced to 2 fs, which decreased significantly the computational speed of the simulations when no elastic bond networks were included.

For each given charge partitioning and configuration, charges were added to the ground state crystallographic PDB structure. The structures were first minimized using the steepest descent method and then initialized with velocities randomly chosen consistent with the temperature. Short molecular dynamics simulations were performed to relax the structures to the equilibrium state. These relaxed structures were used as initial conditions for the center of mass pulling simulations.

GROMACS parameters were set to produce simulations with continuous pulling. That is, the SHAKE algorithm[39] was used to constrain the center of mass distance to a 0.000001 nm tolerance, and this distance was increased by a constant amount at each time step. The resulting pull force needed to maintain each center of mass distance was also collected for later analysis. Continuous pulling simulations were run for a total time of 660 ns using a pull rate of 0.00001 nm/ps. The pull forces are more sensitive than structural parameters, and it was necessary to investigate their convergence, as detailed below.

The convergence of the pull force results was gauged by comparing the predictions from a number of different methods. More specifically, for the M5/M5 charge distribution, three simulations were performed to calculate the pull force. The pull force is the amount of force needed to keep the monomer at a particular COM distance. The integral of the pull force gives the potential of mean force. The first case used the constraint forces from the continuous pulling simulations, as detailed above. Simulations with a faster pull rate of 0.001 nm/ps were also performed for comparison purposes.

The second case used a stepwise pull method. That is, starting from the ground state, the COM distance was increased in steps of 0.15 nm by pulling at a rate of 0.01 nm/ps for 15 ps. Each such pull was followed by a 600 ps simulation during which the center of mass was constrained using the SHAKE algorithm with a 0.000001 nm tolerance. The resulting constraint forces from the last 400 ps (the first 200 ps was allowed for relaxation to occur) of these simulations were time averaged to produce a single force value at that COM distance. This was repeated for 44 steps until the COM distance reached 7.88 nm. In addition to the pull force, the radius of gyration and the RMSD were calculated for the stepwise pull. We chose this method because the all-atom studies[14−16] used a stepwise pull method, although the continuous pull is closer to the dissociation an experimental protein experiences.

The third case used simulations employing umbrella sampling.[40] An umbrella potential force constant of 3300 kJ/(mol nm^2) was used for simulations at a series of COM distances spanning from the ground state dimer distance to 8.4

nm. Each simulation was run for 1800 ps with the last 1600 ps being used for data collection. The resulting histograms were analyzed with the WHAM algorithm as implemented in the GROMACS g_wham utility program.[41] The pull force was then calculated by taking the derivative of the WHAM-generated potential of mean force curve as a function of COM distance.

For each charge partitioning, a number of different parameters were examined using the continuous pulling trajectories. One was the smallest distance between the atoms on one monomer and atoms on the other monomer. This minimum separation was calculated using the GROMACS g_mindist utility. When the minimum separation is small, the monomers have not dissociated, but after dissociation the minimum separation increases. The ground state dimer has a minimum distance of approximately 0.43 nm. Using the minimum separation, it is possible to determine the proportion of the trajectories that have dissociated at each center of mass distance. When the minimum distance for a particular trajectory was greater than 0.8 nm, that trajectory was considered to be dissociated. In addition to the minimum distance, the radius of gyration (R_g) was also calculated. When a protein becomes larger, the radius of gyration increases. The more a protein expands or unfolds, the larger the radius of gyration becomes. Another parameter that can be used to measure changes in the proteins is the root-mean-square deviation (RMSD). RMSD measures the difference between the positions of atoms in the protein and the positions in a reference structure. In this work, the reference structure was chosen to be the structure of the monomer in the ground state dimer.

In addition to structural parameters, the Lennard-Jones and Coulomb contributions to both the intra- and intermolecular energies were examined. The bond, angle, and dihedral angle contributions to the total energy are very small compared to the Lennard-Jones and Coulomb energies, so they are not discussed.

RESULTS AND DISCUSSION

The pull force for the M5/M5 charge partitioning, shown in Figure 3, was calculated using three different methods in order to gauge its convergence. All three methods give the same values for COM distances larger than 7 nm where the pull forces attain a slightly negative value as a result of the Coulomb repulsion between the separated monomers. However, differences appear at smaller COM distances, especially for COM distances between 2 and 3 nm. Here, the continuous pull method with the faster pull rate of 0.001 nm/ps produced the largest pull forces, while the umbrella method produced the smallest ones. This indicates that there is likely some irreversible work present in this continuous pull calculation possibly because the rate of pulling was too large in this COM distance range. This is supported by the fact the stepwise pull calculation produced pull forces closer to the umbrella results. However, the continuous pull with the slower pull rate of 0.00001 nm/ps produced forces much closer to those of the stepwise pull. This slower continuous pull was then used for calculating the structural parameters discussed later. The pull forces from the all-atom study are similar in peak magnitude to the umbrella results, but at distances larger than 5 nm the all-atom pull force is more negative than the coarse-grained pull force. As discussed in ref 15, the all-atom pull force results contain some contributions from irreversible work which have not been removed from the values plotted in Figure 3. Thus, the correct all-atom result is expected to be less than the curve shown. If one takes the umbrella result to be the best one for the coarse-grained calculation, then the pull forces in this case are generally somewhat larger than those corresponding to the all-atom study.

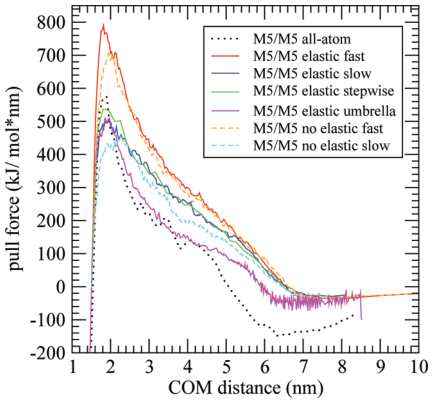

Figure 3. The pull force as a function of center of mass distance for the M5/M5 dimers. The black dotted line is the all-atom pull force. The dashed line is the dimer without elastic network bonds. The solid lines are the dimers with elastic network bonds; the fast continuous pull, slow continuous pull, stepwise pull, and umbrella sampling results are red, brown, green, and magenta, respectively.

The pull force calculated with the same methods (except not with the umbrella sampling) for the M8/M2 dimer can be seen in Figure 4. As in the M5/M5 dimer, the pull force for the slower (0.00001 nm/ps) pull rate is lower than for the 0.001 nm/ps pull rate. The stepwise pull produces similar forces to the slower continuous pull. Unlike the pull force for the M5/M5 dimer, the force for the M8/M2 dimer remains positive for COM distances up to 15 nm. The all-atom results are similar to the coarse-grained slower pull up to a COM distance of 4.5 nm. Trajectories which have dissociated have a very small pull force, while unfolding trajectories which are not dissociated require a significant pull force to move to a larger COM distance. The pull force reported here is the average over both the dissociated and unfolding trajectories, so for COM distances larger than 6 nm the higher pull force for the all-atom method suggests that the all-atom simulations have a smaller percentage of dissociated dimers, implying that there is more unfolding in the all-atom simulations.

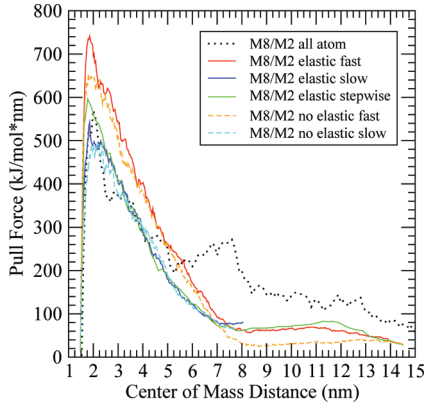

Figure 4. The pull force as a function of center of mass distance for the M8/M2 dimers. The lines have the same meanings as in Figure 3.

Consider now the percentage of dissociated trajectories as a function of COM distance, as shown in Figure 5. The neutral

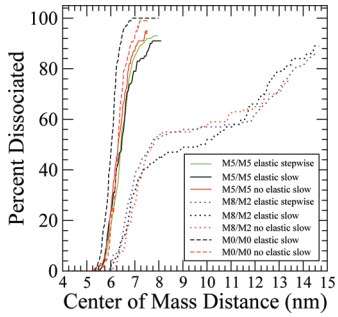

Figure 5. The percentage of the 100 trajectories that have dissociated as a function of the center of mass distance. The solid, dotted, and dashed lines are the M5/M5, M8/M2, and neutral (M0/M0) charge partitionings, respectively. The black and red curves represent slow pulling of the complexes with and without elastic network bonds, respectively. The blue and green lines represent the results of the stepwise pulling.

dimers all dissociate at a similar distance. Between 5.5 and 6.0 nm, the percent dissociated changes rapidly from 0 to 100%. Neutral structures without elastic bond networks tend to dissociate at slightly smaller distances compared with those containing elastic bond networks, but the difference is quite small. The M5/M5 complexes begin dissociating at approximately the same COM distance as the neutral ones, but the rate of dissociation with the COM distance is slightly less than for the neutral complexes. However, in both cases, the steep rise in the curves indicates that the resulting complexes dissociate quickly and with little structural changes.

Contrasting this is the dissociation behavior for the M8/M2 complexes. These complexes begin dissociating at 6 nm and show a strong increase up to a COM distance of 8 nm, at which approximately 50% of the complexes are dissociated. However, after this point, the rate of dissociation drops significantly so that at 14 nm only 80% of the M8/M2 complexes are dissociated. This implies that there are two different behaviors in these complexes. The first, which occurs about 50% of the time, involves dissociation with small but significant structural changes. Complexes exhibiting this behavior have dissociated by the time their COM distances have reached 8 nm. The second, which occurs about 50% of the time, involves dissociation with large structural changes. Complexes exhibiting this behavior likely undergo significant amounts of unfolding during the dissociation process and thus can attain large COM distances before dissociating. Figure 5 also shows that while there is some variation, the dissociation behavior for the M8/M2 structures with and without elastic bond networks is similar.

The behavior seen in Figure 5 can be contrasted with that seen in the corresponding all-atom simulation results, as indicated in Table 1 and Figure 1 of ref 16. For the M5/M5 charge partitioning, the all-atom study showed complexes dissociated over a narrow range of center of mass distances centered at about 5.7 nm, while the neutral ones dissociated at 6.3 nm. Given that the ground state dimer COM distance was 2.0 nm in that study, the neutral and M5/M5 dimers dissociated after being stretched by approximately 4.3 and 3.7 nm, respectively. In the present case, the neutral and M5/M5 dimers do dissociate over a narrow range of COM distances but do so at a distance of approximately 6.0 nm, which represents a stretch of approximately 4.6 nm. In other words, the neutral complexes in the coarse-grained model dissociate after about the same amount of stretching as in the all-atom model. However, the M5/M5 complexes in the coarse-grained model must be stretched to a larger distance before dissociating. The contrast is more noticeable for M8/M2 dimer dissociation. The all-atom results, as seen in Figure 1 of ref 16, show a gradual dissociation process and do not give evidence for different dissociation behavior at short versus long COM distances, as seen in the present Figure 5.

The minimum distance between monomers is expected to increase linearly with an increase in the COM distance. However, for small COM distances, the minimum distance, as shown in Figure 6, remains small and constant. This indicates

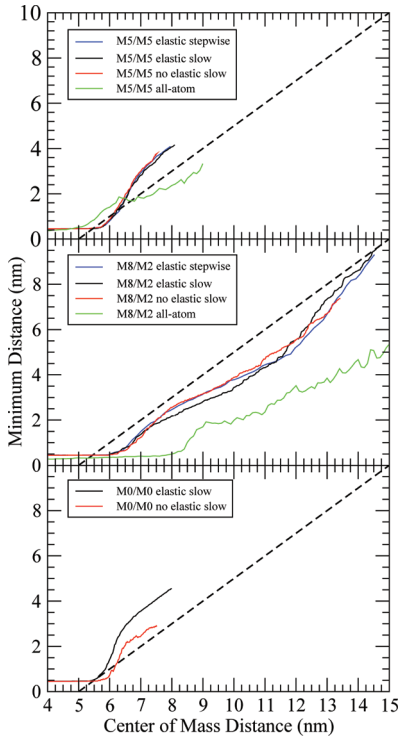

Figure 6. The minimum distance separating the two monomers as a function of center of mass distance. The thick dashed black line has a slope of 1. The black and red curves represent slow pulling of the complexes with and without elastic network bonds, respectively. The blue and green lines represent the results of the stepwise pulling and the all-atom data, respectively.

that the monomers are bound together as a dimer even as the center of masses are pulled apart; that is, the monomers stretch as the COM distance increases. At some point, dissociation occurs, and the minimum distance begins to increase. For the neutral and M5/M5 complexes, this occurs at a COM distance just less than 6 nm, and for the M8/M2 complexes at about 6.5 nm. These distances correspond nicely with the points in Figure 5, at which the dissociation curves begin to rise. For the neutral and M5/M5 complexes, the minimum distance line has a slope greater than 1 just after dissociation at COM distances between 6 and 7 nm. A slope greater than 1 implies that the minimum distance is increasing faster than the rate at which the COM distances are increasing; in other words, the monomers recoil into a more compact form just after dissociation.

Afterward, at about 7.2 nm, the minimum distance line becomes straight and the slope goes to 1, indicating that no further changes in size occur. For the M8/M2 complexes with an elastic bond network, there is a dip in the minimum distance curve at larger COM distances. This is caused by bound complexes in which one of the monomers is unfolding. Such trajectories have a very small minimum distance value, and this lowers the average for the ensemble. As seen in Figure 5, approximately 50% of the complexes undergo this unfolding behavior.

The all-atom study[16] did not measure the minimum distance between monomers, but instead the minimum intermolecular residual pair distance (the smallest distance between amino acids on the two monomers) was calculated. The minimum residual pair distance has slopes of less than 1 after dissociation, indicating structural changes continuing at large COM distances. Most significantly, for no cases was a slope greater than 1 observed for any of the dissociating complexes.

Values of the radius of gyration are shown in Figure 7. For the neutral and M5/M5 charge partitioning, the radius of gyration of the coarse-grained monomers remains approximately constant for all COM distances. In contrast, the all-atom monomers show an increase in radius of gyration for the M5/M5 case starting at a COM distance of 6 nm, that is, after dissociation. For the M8/M2 charge partitioning in both the coarse-grained and all-atom models, the monomer with more charges has a larger increase in radius of gyration than the monomer with fewer charges, resulting from the unfolding of the higher charged monomer. The lower charged monomer has a radius of gyration value essentially the same as seen for the neutral and M5/M5 cases. Interestingly, the increase in radius of gyration is larger for coarse-grained M8/M2 complexes with an elastic bond network compared with those without. However, at COM distances larger than 12 nm, the M8/M2 complexes with elastic bond networks have a curve which begins to decrease. After some investigation, it was found that this occurs because some trajectories which were unfolding in the predissociated state recoiled to a more compact structure after dissociation. This type of refolding after dissociation is not observed in the corresponding all-atom case and is observed to a lesser extent for M8/M2 complexes without elastic network bonds. The stepwise dissociation had slightly higher values for the radius of gyration but showed the same decrease at COM distances larger than 12 nm.

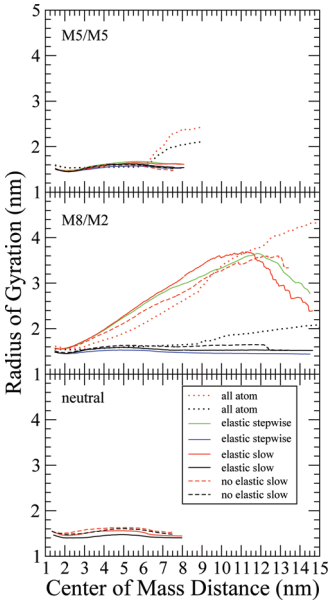

Figure 7. The radius of gyration as a function of center of mass distance for the M5/M5 (top panel) and the M8/M2 (middle panel) charge partitionings and the neutral complex (bottom panel). In all panels, the monomer with the higher and lower charges are shown in red and black, respectively. The solid, dashed, and dotted lines are the complexes with elastic network bonds, the complexes without elastic network bonds, and the all-atom data (M5/M5 and M8/M2), respectively. The green (higher charge) and blue (lower charge) curves are the stepwise pulling results.

A similar conclusion is drawn by examining the values of the RMSD shown in Figure 8. The M5/M5 charge configuration shows an increase in RMSD which then levels off for COM distances larger than 6 nm (when the structure is no longer changing). This is different than the all-atom data, which show the RMSD increasing more after 6 nm. However, at large COM distances, the limiting values are the same for the M5/M5 all-atom and MARTINI models. In the M8/M2 charge configuration, the monomer with more positive charges has a larger increase in RMSD. The all-atom curves initially increase at a slower rate than the corresponding coarse-grained ones but eventually reach comparable values at the largest COM distances. As seen in Figure 7, the coarse-grained RMSD values for the M8 monomers begin to decrease sharply at larger COM distances, again indicating that structures are collapsing to a more compact structure. The neutral monomers have RMSD values slightly smaller than the M5/M5 charge configuration; however both of these charge configurations show the same trend.

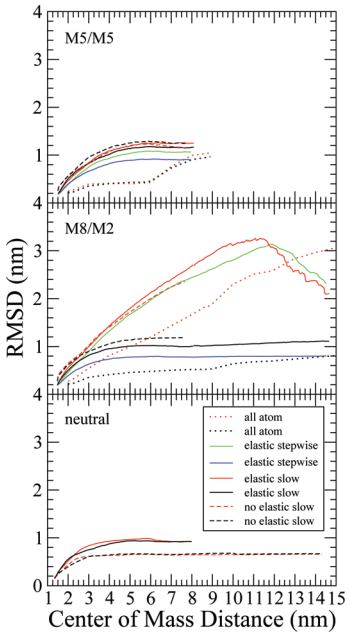

Figure 8. The root-mean-square deviation (RMSD) as a function of the center of mass distance for the M5/M5 (top panel) and the M8/M2 (middle panel) charge partitionings and the neutral complex (bottom panel). The colors and line types have the same meanings as in Figure 7.

For all of the structural parameters, standard deviations were calculated from the set of 100 trajectories at each COM

distance. Because there is an ensemble of structures that contribute to the protein, these standard deviations give a measure of the width of the distribution of the properties. Since all of the trajectories start from a relaxation of the ground state structure, the standard deviation is small at small COM distances (on the order of 5%). As the trajectories propagate, the monomers move away from the ground state and the distributions become wider (standard deviations on the order of 30%).

In the MARTINI force field, some secondary structural elements are imposed using the backbone−backbone bond, angle, and dihedral force constants.[23] For helices, these values are much larger than they are for other secondary structures, so the force field provides a large potential to enforce helical structures. The cytochrome c′ dimer has four helices arranged in a bundle in the ground state. Unfolding can occur in principle through the unbundling of these helices or through the unraveling of individual helices. The former is not hindered by the imposition of secondary structure, while the latter is. In order to better understand the effect of secondary structure on our results, a set of M8/M2 (with local elastic network bonds) simulations was performed with the values of the helical backbone−backbone bond, angle, and dihedral force constants set to 625, 350, and 200 kJ/(mol nm), respectively. These values are half the default ones.

The results of these simulations are shown in Figure 9. Generally, the results are qualitatively the same. However, with the weaker helices, the M8/M2 dimers have a larger percent dissociation and a smaller increase in radius of gyration and RMSD. The larger percent dissociation at small distances (rising from 0% to 60%) implies that a smaller fraction of monomers unfold upon dissociation. This moves the results into worse agreement with the all-atom ones, which show a greater fraction of unfolding, even greater than that seen with the default helical structure parameters. Note that the sharp decrease in RMSD and radius of gyration at larger COM distances is still present in both cases, and the decreases are comparable. Upon examining visually the structures at these large distances, it was found that just before dissociation, they consist of long extended structures, usually with one of the helices being stretched and partially unfolded. After dissociation, these structures compact to globular shapes. Comparable all-atom trajectories also show extended structures before dissociation, some with stretched helical structures. However, after dissociation, the structures remain extended. Caution is required when making comparisons here because the coarse-grained simulations speed up dynamic processes, and in this case, the force-field defined helical parameters additionally increase the rate of helix formation. It is quite likely, given enough time, that the all-atom extended structures would also collapse into globular structures, akin to the coarse-grained ones. The all-atom simulations were not propagated at times long enough for this to happen. However, the fact the all-atom simulations show no sign of compaction while the coarse-grained ones show a great deal of compaction likely indicates that the rate of compaction in the coarse-grained force field is too high relative to the all-atom case.

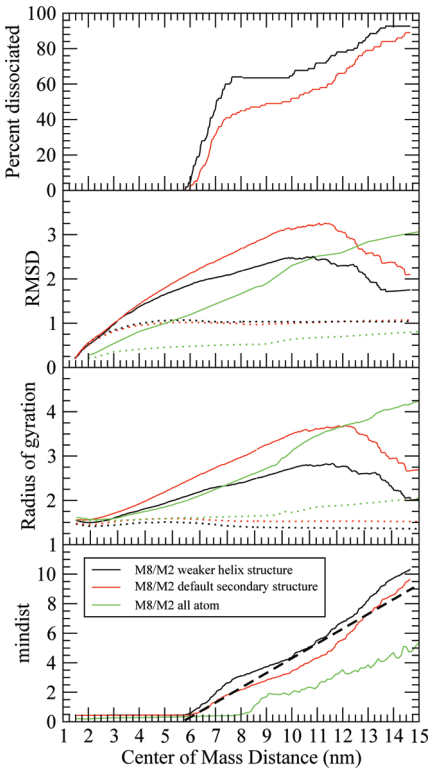

Figure 9. The effect of the secondary structure constraints. The red, black, and green lines represent simulations with the default parameters, simulations with weaker helix structures, and the all-atom simulations, respectively.

Taken together, the results in Figure 9 indicate that the monomers with weaker helices are more compact, which is expected if the rigid helical structure is being somewhat relaxed. This compactness appears to be creating more stable structures, less prone to unfolding. Overall, the relaxation of the helical constraints does not change the qualitative behavior of the complex and, in the case of the percentage dissociation, actually produces results which are further from the all-atom ones. At least in this particular case, the default helical parameters in MARTINI are producing satisfactory results and do not seem to be producing behavior which is inconsistent with the all-atom results, provided detailed quantitative comparisons are not made.

The dissociation behavior of the protein complexes is affected by the balance between the attractive forces within and between the monomers and the repulsive forces caused by the net charges. In order to quantify somewhat this balance, particular components of the potential energy were examined. In the first instance, as seen in Figure 10, the Lennard-Jones intramolecular energy, Coulomb intramolecular energy, and their sum were compared. For all cases, the Lennard-Jones (LJ) intramolecular energy decreases sharply up to a COM distance of 2 nm. Subsequently, the values for the neutral, M5, and M2 monomers become either slowly decreasing or constant up to a distance of about 6 nm, after which point they become constant. In contrast, as a result of unfolding, the energies of the M8 monomers generally increase before becoming essentially constant at larger distances. The M5 and M2 monomers have higher LJ intramolecular energy than the neutral because the positive charges have caused the monomers to expand a bit, thus increasing distances and lowering LJ energy. They have lower LJ intramolecular energy than the M8 monomer because the M5 and M2 monomers have not unfolded while some fraction of the M8 ones have, leading to less intramolecular contacts. The Coulomb intramolecular energy remains approximately constant in all cases except for the M8 monomers, which show a slight decrease with

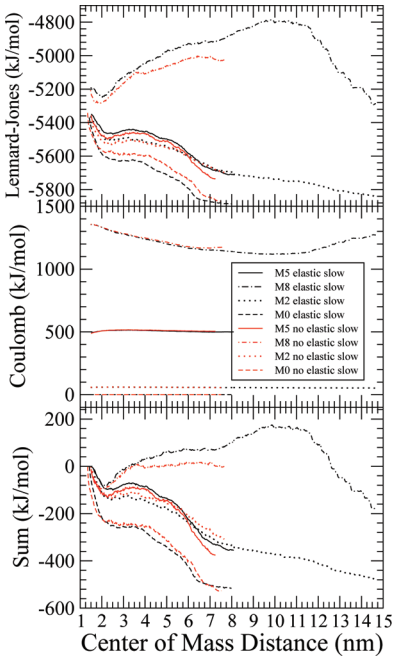

Figure 10. The intramolecular contributions to the LJ (top panel) and Coulomb (middle panel) energies as well as their sum (bottom panel). The sum is scaled so that the ground state energy is 0. In all panels, the solid, dash-dot, dotted, and dashed lines represent the monomers with +5, +8, +2, and 0 charges, respectively. The black and red curves represent complexes with and without elastic network bonds, respectively.

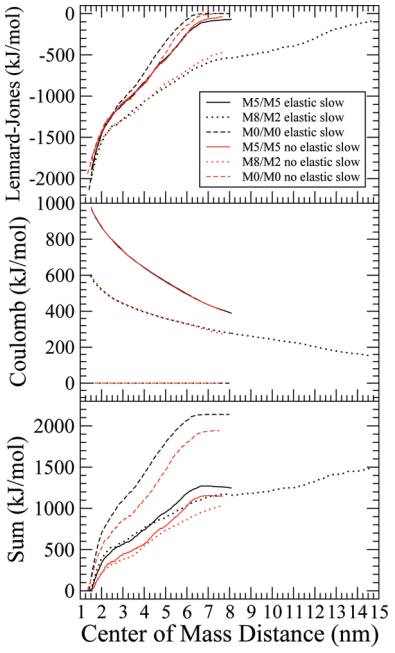

Figure 11. The intermolecular contributions to the LJ (top panel) and Coulomb (middle panel) energies as well as their sum (bottom panel). The sum is scaled so that the ground state energy is 0. In all panels, the solid, dotted, and dashed lines are the M5/M5, M8/M2, and neutral (M0/M0) charge partitionings, respectively. The black and red curves represent complexes with and without elastic network bonds, respectively.

increasing center of mass distance. This is consistent with the fact that the neutral, M2, and M5 monomers show little structural change during the dissociation, while some of the M8 ones unfold, allowing them to lower their intramolecular Coulomb energy. Because the Coulomb contribution is almost constant, the behavior of the total intramolecular energy, as seen in the lower panel of Figure 10, is qualitatively the same as the LJ contribution. Interestingly, at large COM distances, the energies are lower than the corresponding values at small distances, implying that upon dissociation the structures of the monomers change so as to increase their favorable LJ contacts. This is possible because they no longer have the configurational constraints present as part of the dimer.

The Lennard-Jones and Coulomb intermolecular energies are shown in Figure 11. The LJ intermolecular energy is steepest at COM distances less than 2 nm and becomes flat at COM distances greater than 6 nm. This is the same behavior seen for the LJ energies in Figure 4 of the all-atom study.[17] There is very little difference in the LJ intermolecular energy plots between the different charge partitionings. The Coulomb intermolecular energy is expected to have a $1/r$ decay for the M5/M5 and M8/M2 complexes. This smooth decrease in Coulomb energy can be seen in the middle panel of Figure 11. As expected, the M5/M5 has a larger intermolecular Coulomb energy than the M8/M2 because the product of the charges on the monomers is higher in the former case. The relative total intermolecular energies are compared in the bottom panel of Figure 11, where it can be seen that, as expected, the neutral complex has the highest barrier. This barrier is reduced as charges are added to the complex, with the M5/M5 one having the lowest barrier. Note that the coarse-grained model used here does not use partial charges, so its behavior upon dissociation is the same as would be expected for two monopoles separating. The all-atom study did use partial charges, so the intermolecular Coulomb energy reported in ref 16 also contains energy from dipole and higher moments.

In addition to the quantitative comparisons given above, it is possible to compare the coarse-grained and all-atom results on a qualitative level by comparing structures from typical dissociation events. The coarse-grained results are shown in Figure 12 for the M5/M5 and M8/M2 complexes, and these should be compared with the corresponding images in Figure 5 of ref 15 and Figures 5 and 6 of ref 16. Generally speaking, the structural changes are consistent. At a finer level, the

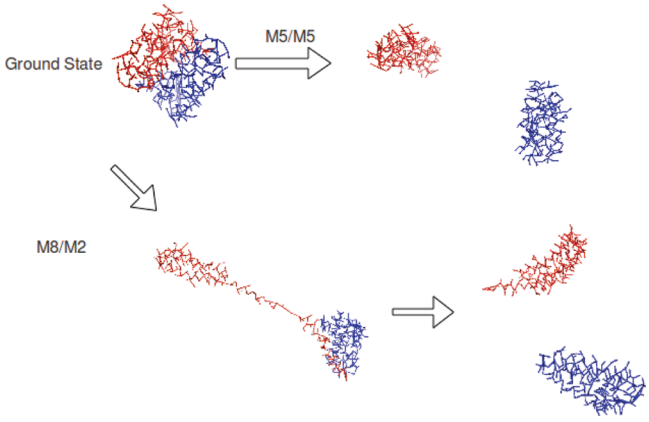

Figure 12. Snapshots of the ground state, M5/M5 (dissociated), and M8/M2 (unfolded) dimers. These images were created using PyMOL.[42] In the M8/M2 dimer, the monomer with more charges is shown on the left.

dissociated monomers for the coarse-grained M5/M5 complex have a more globular shape than the corresponding ones in the all-atom study.

CONCLUSIONS

Taken in their entirety, the results show that the MARTINI force field predicts structures and properties in qualitative agreement with the corresponding all-atom results[15,16] and in many cases in semiquantitative agreement. However, there are several differences worth noting. The radius of gyration values for the dissociated M5/M5 complexes are the same as those before dissociation for the coarse-grained case and do not show the increase seen in the all-atom case. The minimum distance data show that the M5/M5 and neutral coarse-grained complexes contract just after dissociation, a behavior not seen in the all-atom case. This is confirmed by the images in Figure 12 showing a more globular structure for the dissociated M5 monomers. In addition, the pull forces for the M5/M5 dimer dissociation process are consistently higher for the coarse-grained model compared with the all-atom one.

All of these differences indicate that the MARTINI force field appears to have a slightly different balance of attractive and repulsive forces compared to the OPLS-AA/L force field. For the monomers with low charges (neutral, M2, and M5), it is too attractive. This is evidenced by the decrease in radius of gyration after the dissociation and in the minimum distance plot (Figure 6), where immediately after dissociation the slope is greater than 1. For the M8 monomers, the effect of the attractive forces is not seen at smaller distances but is seen in the rapid decrease in radius of gyration (Figure 7) and RMSD (Figure 8) at COM distances greater than 12 nm. Also, while the M8 monomers do show some unfolding behavior, the all-atom pull forces at larger COM distances suggest that the coarse-grained model has less unfolding, which indicates that the force field is too attractive. It is the repulsive charges that help monomers unfold and lower the barrier for dissociation. The MARTINI results are consistent with a model in which the charges are not having the degree of influence as expected from the all-atom results, again indicating that the attractive forces are too large.

The elastic network bonds have only a small effect on the results. However, they significantly increase the time step that can be used. A small number of elastic network bonds in the regions of the protein with the most extended structure have the effect of restricting some fast motions without changing the rest of the protein. As well, the default secondary structure parameters in MARTINI which act to constrain helices especially do not seem to be producing inconsistent results. In other words, the dissociation mechanism is not highly dependent upon the details of the secondary structure changes in the proteins.

The goal of the present study was to determine the suitability of the MARTINI force field for use in molecular dynamics calculations examining the effect of charge migration upon protein complex dissociation. Such a study does not require a highly accurate potential since the dissociation mechanism is expected to be fairly generic and not dependent upon fine interactions. From this perspective, the MARTINI force field should be suitable for such a qualitative study, although for a quantitative study improvements would be desirable. Increasing the number of charges in the system or decreasing the value of the relative dielectric constant would increase the repulsion and thus provide a correction for the balance of attractive and repulsive forces. In a subsequent study, we will employ a charge migration algorithm to study dynamically the dissociation of gas-phase protein complexes.

AUTHOR INFORMATION

Corresponding Author

*E-mail: thachuk@chem.ubc.ca.

Notes

The authors declare no competing financial interest.

ACKNOWLEDGMENTS

This work was supported by a grant from the Natural Sciences and Engineering Research Council (NSERC) of Canada. All computations were performed using WestGrid (www.westgrid.ca)/Compute Canada (www.computecanada.org) computing resources, which are funded in part by the Canada Foundation for Innovation, Alberta Innovation and Science, BC Advanced Education, and the participating research institutions.

REFERENCES

(1) Schwartz, B. L.; Bruce, J. E.; Anderson, G. A.; Hofstadler, S. A.; Rockwood, A. L.; Smith, R. D.; Chilkoti, A.; Stayton, P. S. *J. Am. Soc. Mass Spectrom.* **1995**, *6*, 459−465.
(2) Felitsyn, N.; Kitova, E. N.; Klassen, J. S. *Anal. Chem.* **2001**, *73*, 4647−4661.
(3) Versluis, C.; van der Staaij, A.; Stokvis, E.; Heck, A. J. R.; de Craene, B. *J. Am. Soc. Mass Spectrom.* **2001**, *12*, 329−336.
(4) Felitsyn, N.; Kitova, E. N.; Klassen, J. S. *J. Am. Soc. Mass Spectrom.* **2002**, *13*, 1432−1442.
(5) Benesch, J. L. P.; Sobott, F.; Robinson, C. V. *Anal. Chem.* **2003**, *75*, 2208−2214.
(6) Jurchen, J. C.; Williams, E. R. *J. Am. Chem. Soc.* **2003**, *125*, 2817−2826.
(7) Sobott, F.; McCammon, M. G.; Robinson, C. V. *Int. J. Mass Spectrom.* **2003**, *230*, 193−200.
(8) Jones, C. M.; Beardsley, R. L.; Galhena, A. S.; Dagan, S.; Cheng, G.; Wysocki, V. H. *J. Am. Chem. Soc.* **2006**, *128*, 15044−15045.
(9) Sinelnikov, I.; Kitova, E. N.; Klassen, J. S. *J. Am. Soc. Mass Spectrom.* **2007**, *18*, 617−631.
(10) Wysocki, V. H.; Jones, C. M.; Galhena, A. S.; Blackwell, A. E. *J. Am. Soc. Mass Spectrom.* **2008**, *19*, 903−913.
(11) Benesch, J. L. P.; Ruotolo, B. T.; Simmons, D. A.; Robinson, C. V. *Chem. Rev.* **2007**, *107*, 3544−3567.
(12) Sciuto, S. V.; Liu, J.; Konermann, L. *J. Am. Soc. Mass Spectrom.* **2011**, *22*, 1679−1689.
(13) Csiszar, S.; Thachuk, M. *Can. J. Chem.* **2004**, *82*, 1736−1744.
(14) Wanasundara, S. N.; Thachuk, M. *J. Am. Soc. Mass Spectrom.* **2007**, *18*, 2242−2253.
(15) Wanasundara, S. N.; Thachuk, M. *J. Phys. Chem. A* **2009**, *113*, 3814−3821.
(16) Wanasundara, S. N.; Thachuk, M. *J. Phys. Chem. B* **2010**, *114*, 11646−11653.
(17) Tozzini, V. *Curr. Opin. Struct. Biol.* **2005**, *15*, 144−150.
(18) Yang, L.; Tan, C.-h.; Hsieh, M.-J.; Wang, J.; Duan, Y.; Cieplak, P.; Caldwell, J.; Kollman, P. A.; Luo, R. *J. Phys. Chem. B* **2006**, *110*, 13166−13176.
(19) Jorgensen, W. L.; Tirado-Rives, J. *J. Am. Chem. Soc.* **1988**, *110*, 1657−1666.
(20) Go, N. *Annu. Rev. Biophys. Bioeng.* **1983**, *12*, 183−210.
(21) Sulkowska, J. I.; Cieplak, M. *Biophys. J.* **2008**, *95*, 3174−3191.
(22) Marrink, S. J.; Risselada, H. J.; Yefimov, S.; Tieleman, D. P.; de Vries, A. H. *J. Phys. Chem. B* **2007**, *111*, 7812−7824.
(23) Monticelli, L.; Kandasamy, S. K.; Periole, X.; Larson, R. G.; Tieleman, D. P.; Marrink, S.-J. *J. Chem. Theory Comput.* **2008**, *4*, 819−834.

(24) Berendsen, H. J. C.; van der Spoel, D.; van Drunen, R. *Comput. Phys. Commun.* **1995**, *91*, 43−56.
(25) Van Der Spoel, D.; Lindahl, E.; Hess, B.; Groenhof, G.; Mark, A. E.; Berendsen, H. J. C. *J. Comput. Chem.* **2005**, *26*, 1701−1718.
(26) Hess, B.; Kutzner, C.; van der Spoel, D.; Lindahl, E. *J. Chem. Theory Comput.* **2008**, *4*, 435−447.
(27) Baron, R.; de Vries, A. H.; Hunenberger, P. H.; van Gunsteren, W. F. *J. Phys. Chem. B* **2006**, *110*, 8464−8473.
(28) Baron, R.; de Vries, A. H.; Hunenberger, P. H.; van Gunsteren, W. F. *J. Phys. Chem. B* **2006**, *110*, 15602−15614.
(29) Baron, R.; Trzesniak, D.; de Vries, A. H.; Elsener, A.; Marrink, S. J.; van Gunsteren, W. F. *ChemPhysChem* **2007**, *8*, 452−461.
(30) Yefimov, S.; van der Giessen, E.; Onck, P. R.; Marrink, S. J. *Biophys. J.* **2008**, *94*, 2994−3002.
(31) Euston, S. R. *Biomacromolecules* **2010**, *11*, 2781−2787.
(32) Sengupta, D.; Marrink, S. J. *Phys. Chem. Chem. Phys.* **2010**, *12*, 12987−12996.
(33) Schfer, L. V.; de Jong, D. H.; Holt, A.; Rzepiela, A. J.; de Vries, A. H.; Poolman, B.; Killian, J. A.; Marrink, S. J. *Proc. Nat. Acad. Sci.* **2011**, *108*, 1343−1348.
(34) Singh, G.; Tieleman, D. P. *J. Chem. Theory Comput.* **2011**, *7*, 2316−2324.
(35) Milani, A.; Casalegno, M.; Castiglioni, C.; Raos, G. *Macromol. Theory Simul.* **2011**, *20*, 305−319.
(36) Ren, Z.; Meyer, T.; McRee, D. E. *J. Mol. Biol.* **1993**, *234*, 433−445.
(37) Nosé, S. *J. Chem. Phys.* **1984**, *81*, 511−519.
(38) Periole, X.; Cavalli, M.; Marrink, S.-J.; Ceruso, M. A. *J. Chem. Theory Comput.* **2009**, *5*, 2531−2543.
(39) Kräutler, V.; van Gunsteren, W. F.; Hünenberger, P. H. *J. Comput. Chem.* **2001**, *22*, 501−508.
(40) Torrie, G. M.; Valleau, J. P. *Chem. Phys. Lett.* **1974**, *28*, 578−581.
(41) Hub, J. S.; de Groot, B. L.; van der Spoel, D. *J. Chem. Theory Comput.* **2010**, *6*, 3713−3720.
(42) DeLano, W. L. The PyMOL Molecular Graphics System; DeLano Scientific LLC: San Carlos, CA, 2010. http://www.pymol.org (accessed Mar. 2012).